Mid-infrared Polaritonic Coupling between Boron Nitride Nanotubes and Graphene

Xiaoji G. Xu,[†,⊥] Jian-Hua Jiang,[‡,⊥] Leonid Gilburd,[†] Rachel G. Rensing,[‡] Kenneth S. Burch,[‡] Chunyi Zhi,[§] Yoshio Bando,[∥] Dmitri Golberg,[∥] and Gilbert C. Walker*[,†]

[†]Department of Chemistry, University of Toronto, Toronto, Ontario M5S 3H6, Canada, [‡]Department of Physics, University of Toronto, Toronto, Ontario M5S 1A7, Canada, [§]Department of Physics and Material Science, City University of Hong Kong, 83 Tat Chee Avenue, Kowloon Tong, Hong Kong, China, and [∥]World Premier International (WPI) Center for Materials Nanoarchitectonics (MANA), National Institute for Materials Science (NIMS), Tsukuba, Ibaraki 305-0044, Japan. [⊥]These authors contributed equally.

ABSTRACT Boron nitride (BN) is considered to be a promising substrate for graphene-based devices in part because its large band gap can serve to insulate graphene in layered heterostructures. At mid-infrared frequencies, graphene supports surface plasmon polaritons (SPPs), whereas hexagonal-BN (*h*-BN) is found to support surface phonon polaritons (SPhPs). We report on the observation of infrared polaritonic coupling between graphene SPPs and boron nitride nanotube (BNNT) SPhPs. Infrared scattering type scanning near-field optical microscopy is used to obtain spatial distribution of the two types of polaritons at the nanoscale. The observation suggests that those polaritons interact at the nanoscale in a one-dimensional/two-dimensional (1D/2D) geometry, exchanging energy in a nonplanar configuration at the nanoscale. Control of the polaritonic interaction is achieved by adjustment of the graphene Fermi level through voltage gating. Our observation suggests that boron nitride nanotubes and graphene can interact at mid-infrared frequencies and coherently exchange their energies at the nanoscale through the overlap of mutual electric near field of surface phonon polaritons and surface plasmon polaritons. Such interaction enables the design of nano-optical devices based on BNNT-graphene polaritonics in the mid-infrared range.

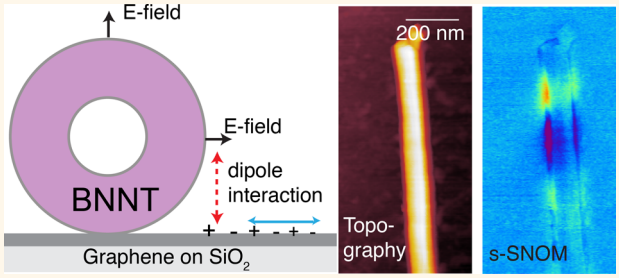

KEYWORDS: boron nitride · graphene · nanotube · phonon polariton · plasmon · near-field · s-SNOM

Surface polaritons are hybrids of bound electromagnetic waves and charge oscillations. Typically, surface plasmon polaritons (SPPs) are mainly supported by noble metals and reside in the visible and near-infrared frequencies,[1,2] whereas surface phonon polaritons (SPhPs) are supported by polar materials, such as silicon carbide,[3−6] ZnO,[7] GaAs,[8] and boron nitride (BN),[9−12] at the mid-infrared frequencies.[13] Materials enabling high-field confinement of optical and infrared fields well below the diffraction limit through surface polaritons are building blocks of nanophotonic devices.[14] A systematic understanding of the plasmon polartion interactions at the visible range has been achieved through years of research; in comparison, research on mid-infrared polaritons is at its nascent stage. In this paper, we report an investigation of graphene plasmon polaritons and boron nitride nanotube (BNNT) surface phonon polaritons and our observation of the interaction between them in the mid-infrared frequency range in a nonplanar geometry. We also use electrical gating of graphene plasmons to control the photonic responsivity of a graphene−BNNT nanocomposite. The results are theoretically modeled and suggest active infrared devices integrating these materials.

Doped graphene, with gate-tunable carrier density, supports plasmons in a wide range of mid-infrared frequencies.[15−19] Hexagonal boron nitride (*h*-BN) forms various structurally analogous forms to carbon allotropes, such as one-dimensional nanotubes and two-dimensional sheets.[20−22] A strong phonon resonance of *h*-BN leads to a negative region of the real part of dielectric function,[23] which is capable of supporting surface phonon polaritons (SPhPs).[13] Boron

* Address correspondence to gwalker@chem.utoronto.ca.

Received for review July 23, 2014 and accepted October 26, 2014.

Published online 10.1021/nn504093g

nitride SPhPs at the mid-infrared frequency have been observed in BN sheets[9−11] and BNNTs.[12] BNNTs have a variety of mechanical, energy, thermal, and biological applications,[24−28] which have not taken advantage of BNNTs' phonon polaritons. Both graphene plasmons and BN phonon polaritons are highly confined, with polariton wavelengths on the order of a hundred[12] to several hundreds of nanometers, and they also share the same range of frequencies in the mid-infrared. Such a match of wave-vector and frequency opens the possibility of coupling and hybridization of the two types of surface waves, confined in suitable geometries. The coupling and mode hybridization between graphene plasmons and optical phonons has been studied in a stacked-layer geometry of SiO_2[29,30] and SiC.[31,32] A recent study of nanoscale patterned graphene on monolayer BN with far-field FTIR suggests strong coupling between graphene plasmons and *h*-BN optical phonons that allows efficient energy transfer between plasmon and phonon states.[10] In such a stacked-layer geometry, the in-plane electric field generated by lattice vibrations (phonons) induces charge oscillations in the proximate graphene layer and vice versa. Such a mechanism leads to mode hybridization and level splitting of *h*-BN phonons and graphene plasmons and formation of hybrid surface−phonon−plasmon−polaritons.[10]

However, there are situations where graphene and BN are not always in immediate contact with each other and may have an angle between their surfaces. Would spatially separated, nonparallel BN and graphene interact at the mid-infrared frequencies? More specifically, BNNT has a nonplanar geometry, where the BN surface is not parallel to the graphene plane. The polariton hybridization model that has been applied to the parallel stacked-layer geometry is no longer applicable to BNNT with graphene. Would the SPhPs of BNNT interact with the graphene plasmons? What would be the likely mechanism?

RESULTS AND DISCUSSION

To experimentally find the answers to these questions, we make nanoscale measurements of the infrared interactions between BNNT and graphene when the materials are placed in proximity. Infrared scattering type near-field optical microscopy (s-SNOM) is used to directly map surface polaritons of BNNTs/graphene. The 10 nm spatial resolution of s-SNOM reveals the locations of polaritons at a resolution below the diffraction limit. Infrared s-SNOM has been used in various occasions for mapping surface plasmons, phonons, and electric fields on the nanoscale.[3,33−35] Multiwall BN nanotubes can be synthesized by a chemical vapor deposition method.[36−38] In our study, we use the synthesis method described in previous paper.[36]

BNNTs were placed on top of p-doped graphene on a SiO_2/Si substrate. Then s-SNOM images with infrared near-field responses of BNNTs and graphene were obtained. Figure 1a shows the AFM topography of a nanotube of 80 nm external diameter (70 nm vertical, 90 nm lateral dimension). The $\pi/2$ phase controlled homodyne technique[39] was used to obtain the near-field image of the nanotube. It allows extraction of near-field signal that is $\pi/2$ out of phase from the phase reference substrate, in our case, the graphene substrate that is far from the BNNT. The $\pi/2$ near-field image of the BNNT and graphene was obtained as shown in Figure 1b. The SPhPs are present in BNNT at 1400 cm^{-1}, where the real part of dielectric BN function is negative.[12,23] However, there is a noticeable "halo" on the near-field image, *i.e.*, a graphene near-field response at the vicinity of the BNNT (marked by arrows). The strong localized halo is observed about 300 nm from the tube terminal, coincident with a low amplitude phonon polariton of the nanotube. Figure 1c shows the profile of the $\pi/2$ near-field response (blue curve) along the white dashed line in Figure 1b and AFM topography (black curve) across the nanotube. From this profile, the decay range of the halo is found to be 40 nm. While we have observed such halo responses on BNNT/graphene samples under different homodyne conditions, we have not observed such a halo response from BNNTs on a smooth gold substrate,[12] which suggests a relation between the halo responses and graphene dielectric properties. In addition, such a localized halo response is not observed for graphene substrate when the frequency is outside of the BNNT SPhP active frequency region (see Figure S1, Supporting Information), which indicates the essential role of SPhPs in the halo responses. Measurements of additional BNNT/graphene responses at different frequencies are provided in Figure S2d−f (Supporting Information).

Figure 1e shows a BNNT terminal studied with in-phase homodyne condition at 1405 cm^{-1} (the topography is shown in Figure 1d). The in-phase homodyne is achieved by maximizing the near-field signal from the graphene substrate. It reads out the near-field responses that are of the same phase as those from the flat graphene substrate, which under the in-phase homodyne condition exhibits non-zero near-field response. Complementary to $\pi/2$ phase homodyne, the in-phase homodyne measurement allows the identification of phase relation of the halo responses from the graphene that are along the BNNT shaft. If one uses the near-field signal from the graphene substrate far from the BNNT as a reference point, there is a positive intensity region of the halo response at 190 nm from the tube terminal and a negative intensity region at 340 nm from the terminal of the BNNTs. The near-field response profiles across the positive intensity location (black dashed line in Figure 1e) and negative intensity location (white dashed line in Figure 1e) are shown in Figure 1f. The decay lengths of the positive halo and

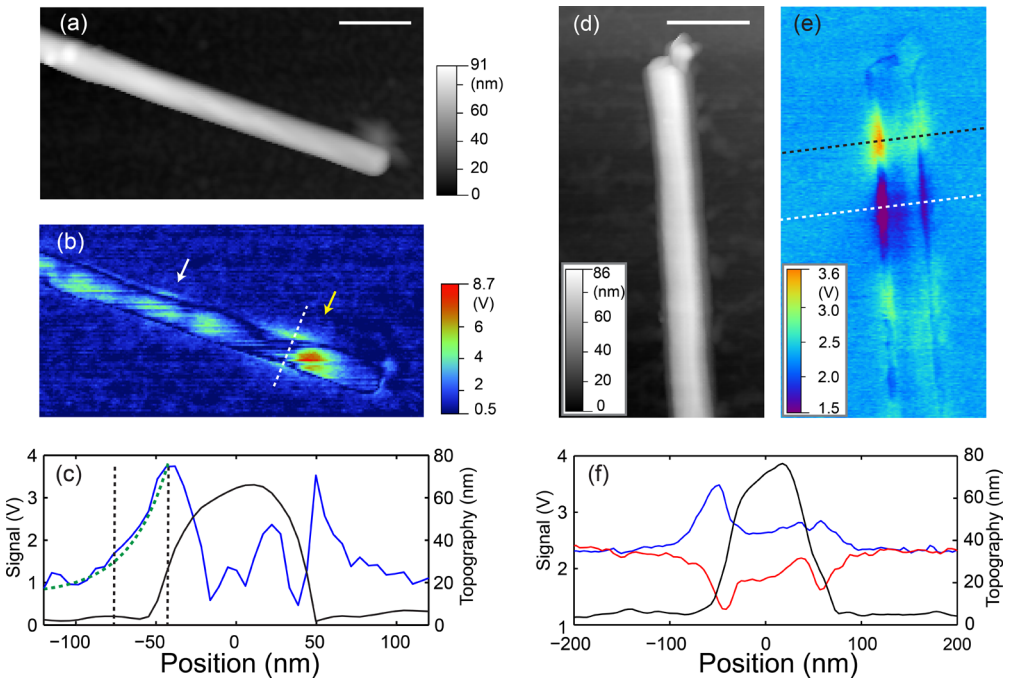

Figure 1. Distribution of near-field responses near the BNNT shaft. (a) AFM topography of the BNNT terminal. White scale bar is 200 nm. (b) Near-field image of the terminal of the BNNT exhibiting a halo in the vicinity of the BNNT (π/2 out-of-phase homodyne amplification with 1400 cm^{-1} IR light). The halo is due to the presence of graphene plasmons. The graphene plasmon is stronger near the terminal end of the BNNT, indicating strong coupling between surface phonon polaritons and graphene plasmons. (c) Profile across the terminal of the BNNT marked by white dashed line in (b) shows that the near-field response is delocalized out of the BNNT tube (blue curve). A profile of AFM topography is shown as a reference (black curve). From the profiles, a plasmon coherence length is obtained to be 40 nm. Numerical simulated near-field curve (green dashed curve) is shown in comparison to the near-field response (overlaid to the left side). (d) Topography of another nanotube. (e) Near-field image of the BNNT in (d) with in-phase homodyne amplification with 1405 cm^{-1} IR light. It exhibits positive and negative regions of near-field response along the nanotube. (f) Profiles across two locations. Blue curve corresponds to the black dashed line in (d); red curve corresponds to white dashed line in (e). Topography profile of the nanotube is shown as the black curve.

negative halo that are perpendicular to the BNNT are ~35 nm, comparable to what is seen in Figure 1c.

What is the nature of the observed halo in graphene near BNNTs? Is it a manifestation of graphene plasmons? The doped graphene substrate is capable of supporting plasmons, according to our observation of similar responses of the graphene plasmons from the boundary at this wavelength (Figure S3, Supporting Information). One of the characteristics of graphene plasmon is its dependence on carrier density, which can be controlled through voltage gating. To test the behavior of the halo, we performed voltage gating experiments to address these questions. Voltage gating allows control of electric and optical properties of graphene through adjusting the Fermi level with respect to its charge neutrality point; such gating can control the ability of graphene to support plasmons.[16−18] In our experiment, we apply a gate voltage between graphene and its insulating SiO_2 substrate to investigate the behavior of the graphene halo response near a BNNT. Figure 2a shows the topography of a BNNT on graphene. When a positive gate voltage of 60 V is applied, the π/2 graphene halo response near the BNNT terminal is suppressed (Figure 2b, marked by the white arrow) compared to zero gate voltage (Figure 2c). Oppositely, a gate voltage of −60 V increases the halo response in graphene (Figure 2d). The profiles of halo responses at the BNNT terminal at different gate voltages are shown in Figure 2e. A trend of increasing halo near-field amplitude and ranges is clearly seen as more negative gate voltages are applied. A conductance measurement (Figure 2f) confirms the relation between gate voltage and graphene conductivity. As a positive gate voltage is applied, the conductance drops as the Fermi level approaches the charge neutrality point of the graphene. It is known that the ability to support plasmon response decreases with an increase of the Fermi level for hole-doped graphene.[17,18] Plasmon damping is reduced when the Fermi energy $|E_F| > (\hbar\omega)/2$, leading to greater extension length into the graphene, parallel to the graphene substrate, and increasing plasmon range. The graphene halo response that we have clearly observed has similar dependence on graphene Fermi energy as graphene plasmons. The short-range halo response could be attributed to a graphene plasmon in a high loss regime for SiO_2 hybridized graphene.[30]

However, there is a key feature that cannot be simply explained by assuming that the halo responses are graphene plasmons alone. In s-SNOM studies of

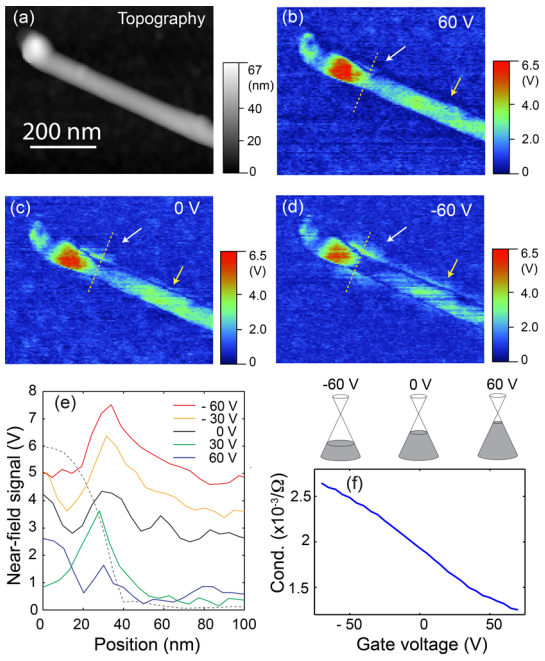

Figure 2. Voltage gating of graphene substrate influences the graphene plasmon in proximity to a BNNT. (a) AFM topography of a BNNT on graphene/SiO_2/Si substrate. The white scale bar is 200 nm. (b) Near-field image of the BNNT on graphene substrate at 60 V gate voltage with 1405 cm^{-1} IR excitation, with out-of-phase (π/2) homodyne condition. (c) Near-field image of the BNNT at 0 V gate voltage and (d) at −60 V gate voltage. The white and yellow arrows of (b−d) indicate locations of the graphene plasmon due to the coupling with BNNT phonon polaritons. (e) Profiles of the near-field images from −60 V gate voltage to 60 V gate voltage with increment of 30 V. (AFM topography is shown as dashed curve. The response is offset vertically for clarity.) (f) Measured conductance vs gate voltage of the graphene on SiO_2/Si substrate. Positive gate voltage brings the Fermi level to the charge neutrality point. The overall measurement shows a decrease of phonon polariton coupling to graphene plasmon as the Fermi level of graphene is approaching its charge neutrality point by the voltage gating.

graphene plasmons,[17,18] the sharp metallic tip is thought to be the main excitation source to launch plasmons in graphene; the direct far-field momentum coupling to planar graphene is negligible due to poor phase matching geometry. The near-field plasmon contrast of graphene is generated by the reflection of tip-generated plasmons at boundaries of discontinuous electrical properties. A BNNT would simply serve as such a boundary. If this were the case for the observations in Figures 1 and 2, one would expect *uniform* graphene responses along the BNNT.[17] The response from the BNNT terminal region would be the same as the response from the region near the stem, *e.g.*, location marked by the white arrow in Figure 1b (see Figure S2b,c in the Supporting Information for additional experimental observations of a BNNT serving as a simple reflection boundary when the infrared frequency is lower than the SPhP frequency of the BNNT). However, the near-field measurement clearly shows a nonuniform graphene halo response along the BNNT. There are discernible stronger responses arising from the location near the nanotube terminal end than from other locations along the tube stem. Furthermore, the in-phase homodyne near-field image of Figure 1e shows increase and decrease of graphene near-field response along the sides of the nanotube due to constructive and destructive interferences, suggesting spatial coherence, *i.e.*, an evolving phase relation of the graphene response from the vicinity along the BNNT, which cannot be interpreted by simple boundary reflection. Such behaviors suggest that BNNT is not just a barrier. Instead, there are dynamic degrees of freedom in the BNNT that couple with graphene plasmons.

What is the specific field coupling mechanism between BNNTs and graphene? One way is to describe it as interactions between independent quasi-particles of SPhPs and SPPs. In the SPhPs of BNNT, the polaritonic energy is partitioned between phonon transverse oscillations and bound electromagnetic fields. In the case of graphene SPPs, the polaritonic energy is distributed between the longitudinal electron motions and bound electromagnetic fields. When the BNNT and graphene are close in proximity and in the proper geometry, the bound electromagnetic field component of the BNNT SPhP and the graphene surface plasmon efficiently overlap, allowing the energy to flow from the BN phonon oscillations to graphene charge oscillations, and *vice versa*. Such energy flow is the cause of coupling and leads to the spatial modulation of graphene plasmon responses at the BNNT SPhPs' spatial frequency along the side of the BNNT. The experimental observation of the halo response is explainable in this independent quasi-particles interaction model. Figure 3a shows the sequence of such interactions: when the metallic probe tip is on graphene near a BNNT, it first excites the graphene plasmons, and then plasmons propagate in graphene to reach the BNNT/graphene interface. Near the interface, the electric field component of longitudinal graphene plasmon is aligned with the electric field component of BNNT transverse phonon polariton, allowing efficient transfer from graphene plasmons to BNNT SPhPs through dipole interactions (Figure 3b). After that, SPhPs propagate along the BNNT and are reflected back at the terminal of the nanotube. The reflected SPhPs travel back and are converted back into graphene plasmons and coherently add to the directly tip-launched plasmons, leading to a modulation of near-field signals. As the phase of SPhPs evolves while they travel along the BNNT, the total plasmon responses under the metallic tip exhibit spatial variations along the stem of the BNNT in accordance with the SPhP's propagation wave-pattern. The phase difference between the constructive and destructive interference between the reflected and directly tip-launched waves is π/2, which corresponds to 150 nm separation between the locations between positive signal (190 nm from the terminal) and negative signal

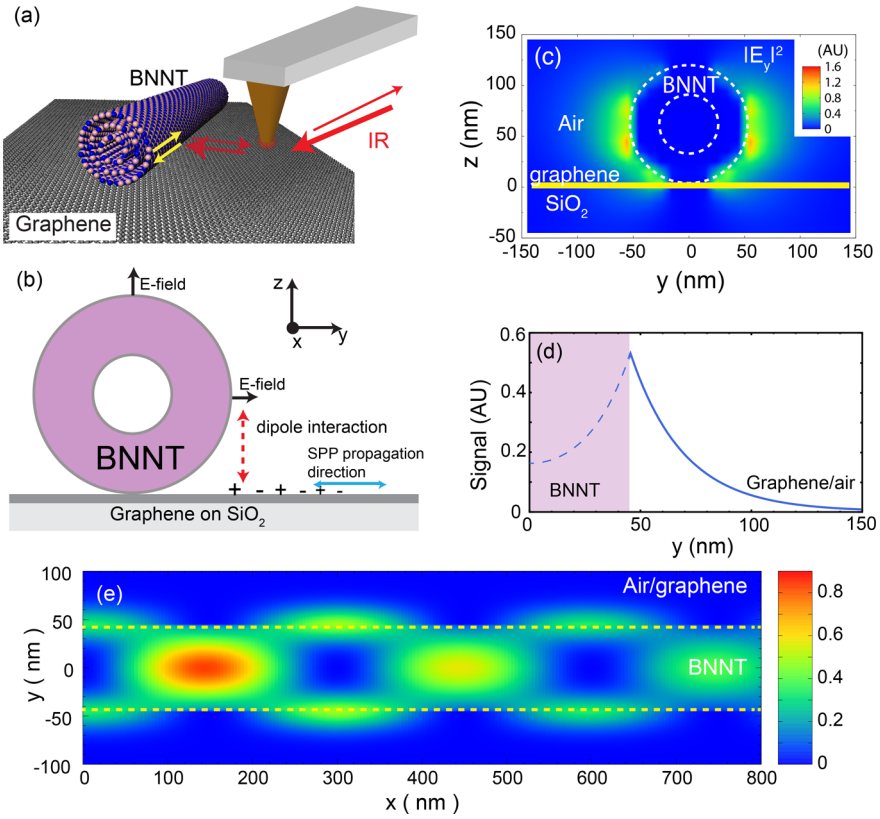

Figure 3. Scheme of near-field interaction and signal generation. (a) AFM probe tip is on graphene near a BNNT. (b) Scheme of electric field of a BNNT interacting with a monolayer of doped graphene. The electric field of the transverse phonon polaritons at the side of BNNT is parallel with the dipole oscillation of graphene surface plasmon polaritons, which is longitudinal. The parallel geometry leads to efficient coupling between BN SPhPs and graphene plasmons. (c) The finite domain time domain simulation of the amplitude square of the electric field distributions along the y direction of the BNNT/graphene cross section. The dashed circles show the diameter and hollow core of the BNNT. (d) Simulation of hybrid graphene/BN plasmon-phonon polariton and its interaction range. This hybrid mode decays rapidly from the BN-graphene interface, which agrees with the experimental observation in Figure 1. (e) Simulated polariton intensities in the $x-y$ plane, which shows periodicity along the x-direction (BNNT starts at $x = 0$), and is of out of phase between pure BN SPhPs and hybridize plasmon-phonon polaritons. To illustrate that the SPhPs are almost reflected by the terminal of BNNT, we take the reflection coefficient as $r = 1$. In comparison, the reflection coefficient for the plasmon-phonon polariton is taken as $r = 0.7i$ in the calculation to account for the shift of peak and reduced signal intensity. The results plotted in (d) (e) are the calculated intensity of the reflected wave which reproduce the main features of the observation in Figure 1.

(340 nm from the terminal) in Figure 1e. The observation gives the polariton wavelength λ_{SPhP} to be 600 nm, which is deduced from 2π phase for a full period, if 150 nm corresponds to $\pi/2$ phase. The polariton wavelength agrees with a correlation of the BNNT SPhP wavelength λ_{ph} with the tube diameter (see Figure S4 in the Supporting Information for BNNT diameters vs effective indices). The interaction model explains the shift of localized halo location at different infrared frequencies Figure S2d–f, Supporting Information), as the halo position is correlated with the SPhP wavelength.

To confirm the above conjecture on the coupling between the BNNT SPhPs and graphene plasmons, we performed a finite-difference time-domain (FDTD) calculation of the cross-section of the BNNT/graphene structure assuming an infinitely long BNNT on top of graphene. The distribution of the electric field along the y direction for the eigenmode with frequency 1400 cm^{-1} for a BNNT with an outer diameter of 100 nm and a hollow center 20 nm in diameter is plotted in Figure 3c. The electric field component parallel to the graphene plane and perpendicular to the BNNT is strongest at the sides of the BNNT, which is consistent with our proposed interaction scheme, shown in Figure 3b. This is supported by numerical simulation (for more results, see Figure S6, Supporting Information). However, a full three-dimensional FDTD simulation for long BNNTs is computationally cumbersome due to the large disparity in geometric feature size, namely, the length (>1 μm) and the diameter (<100 nm) of the nanotube. Therefore, we use the analytic forms of the hybridized electromagnetic fields, which are analogous to surface plasmon polariton theory,[34] to describe the essence of the polaritonic coupling between SPhPs in the BNNT and plasmons in graphene

$$\bar{E}_i = (E_{ix}, E_{iy}, 0)e^{-k_i||y|-\frac{d}{2}|}e^{-j(qx-\omega t)} \quad (1a)$$

$$\bar{H}_i = (0, 0, H_{iz})e^{-k_i||y|-\frac{d}{2}|}e^{-j(qx-\omega t)} \quad (1b)$$

where $k_i = (q^2 - \epsilon_i \omega^2/c^2)^{1/2}$ with q being the wave-vector along the BNNT, i is the label for different materials ($i = 1$ for BN, $i = 2$ for graphene, and $i = 3$ for the air), d is the diameter of the BNNT, and $-j$ is the imaginary unit. The x-direction is along the BNNT, and the z-direction is perpendicular to the substrate and direction x (Figure 3b). The y direction is defined as perpendicular to the BNNT and parallel to the graphene plane. The $x-z$ plane is chosen to contain the central axis of the BNNT. Such an analytical form allows us to calculate the s-SNOM signal which considers the joint field contribution of the BNNT SPhPs and graphene plasmons in the system. The dielectric function of BNNT is expressed as

$$\epsilon_1(\omega) = \epsilon_\infty + \frac{s^2}{\omega_{TO}^2 - \omega^2 + i\omega\gamma} \quad (2)$$

where the parameters ω_{TO} = 1363 cm^{-1} and γ = 27.5 cm^{-1} are extracted from FTIR measurements of BNNTs (see the Supporting Information, Figure S5) and $\epsilon_\infty = 4.95$ and $s^2 = 3.5 \times 10^6$ cm^{-2} are taken from Geick *et al.*,[23] which are deduced from experimental IR data on bulk *h*-BN. Those parameters have been used in previous FDTD calculation of SPhPs in BNNT which achieved good quantitative agreements with experimental measurements,[17] although the dielectric properties of nanotubes are different from the bulk material when the diameter of the nanotube is very small (diameter < 5 nm).[40] The dielectric function of graphene $\epsilon_g(q, \omega)$ is calculated on the basis of the literature[41] (Figure S7, Supporting Information). Similarly, the field configuration between the BN and air at the top of the BNNT can be modeled as

$$\bar{E}_i' = (E_{ix}, 0, E_{iz}) e^{-k_i|z|} e^{-j(qx - \omega t)} \quad (2a)$$

$$\bar{H}_i' = (0, H_{iy}, 0) e^{-k_i|z|} e^{-j(qx - \omega t)} \quad (2b)$$

Here, the material label $i = 1$ for BN and $i = 3$ for the air. Equations 2a and 2b account for the SPhPs between the top part of BN and the air, whereas eqs 1a and 1b account for the hybrid SPhP and graphene plasmons at the side of BNNT above graphene. The calculated s-SNOM signals are plotted in parts d and e of Figures 3, which account for wave propagation and decay along the paths illustrated in Figure 3a. The calculated decay range of the hybrid mode in Figure 3d shows good agreement with the measured data (see Figure 1c, green dashed curve for the calculated curve at the left side of the BNNT). The calculated results in Figure 3e also agree well with the s-SNOM signals in Figure 1b.

Effective polaritonic coupling between SPhPs in BNNT and plasmons in graphene is observed in the nonplanar structures with the electromagnetic field configurations that allow efficient near-field coupling. In comparison to *h*-BN/graphene heterostructure, the BNNT/graphene structure has several favorable traits for nanophotonics devices. First, BNNTs allow modest but intrinsic wave-guiding capability due to its one-dimensional nature. Second, BNNTs possess high *lateral* field confinement as demonstrated by their high effective indices.[12] Furthermore, the geometry of nanotubes allows adjustment of the wave characteristics and versatile control of polariton wavelength (momentum), and the control of the geometry of the BNNT can be done during large-scale chemical synthesis, rather than time-consuming nanofabrication.

The existence of mid-IR energy coupling between 1D material, *i.e.*, the BN nanotube, and 2D material, *i.e.*, graphene, enables a new design principle for graphene-based devices relying on the unique BN or other phonon active materials properties. For example, boron nitride is an insulator that does not allow free electron flow. Therefore, one might use BNNTs as waveguides to pass energies in the form of surface phonon polaritons between two graphene patches without affecting the Fermi levels of individual graphene areas, to serve as an energy conduit without conducting electrons. This would not be possible by using electrically conducting waveguides. In addition, the graphene plasmons have short lifetimes of several tens of femtoseconds due to their large plasmon line width.[30] On the other hand, phonon polariton media have modal lifetimes dependent upon the optical phonon lifetime, as in the case of *h*-BN. The lifetime of BNNT phonon polaritons is hence estimated to be between ~1 and several picoseconds. The existence of mutual energy transfers between graphene and BN means that the phonon polariton can serve as energy storage for graphene plasmons to prolong their lifetime at mid-infrared frequencies.

Another interesting potential application is the use of electrical gating of graphene that supports BNNT to create a multilevel system that could support a population inversion and an IR gain medium. The use of a (quasi) periodic substructure of gold has been shown to create a bandgap that governs the frequency of the surface phonon polariton of BNNTs.[12] These elements might be combined to create a distributed feedback of gain along the edge of the nanotube.

2D *h*-BN has been identified as potentially an ideal substrate and component for graphene electronics.[42−45] Brar *et al.* showed that strong coupling exists between graphene and *h*-BN sheets in stacked-layer geometry in the mid-infrared regime.[10] Here, we show that at the side of BNNT there exists polaritonic coupling with graphene substrate. Similarly, such coupling should also exist between *h*-BN and graphene, if they have an angle between their nearby surfaces, which allows field overlap between longitudinal graphene plasmons and transverse BN phonon polaritons. These results indicate new opportunities for mid-infrared device design and engineering based on polaritonic coupling between graphene and BN.

CONCLUSION

In summary, we have observed infrared polaritonic interaction between graphene plasmons and surface phonon polaritons of BNNT with the means of infrared nanoimaging. The control of the polaritonic interaction is achieved by adjustment of the graphene Fermi level through voltage gating. The underlying mechanism of the polaritonic coupling between BNNTs and graphene is found to be the mutual overlap between electric field components of transverse BN SPhPs and longitudinal graphene plasmons. Our result suggests a polariton interaction scheme between graphene plasmons and boron nitride surface phonon polaritons in a nonplanar configuration, which can be used for designing infrared nanodevices involving graphene and BN materials.

MATERIALS AND METHODS

Materials. The multiwalled boron nitride nanotubes (BNNTs) were synthesized by using high-temperature chemical vapor deposition (CVD) synthesis in an induction furnace. More details may be found in literature.[36] MgO, SnO, and B powders at a weight ratio of 7:150:30 were thoroughly mixed, placed in a BN crucible, and heated by induction currents up to 1400−1500 °C in a flow of an Ar carrying gas and a NH_3 reactive gas. The obtained snow-white BN product was purified by annealing in Ar atmosphere at 1900 °C in the induction furnace. CVD-synthesized monolayer graphene on Si/SiO_2 (Gratom-M Bluestone) was purchased commercially. The thickness of the SiO_2 insulating layer between the graphene and Si substrate was 285 nm. BNNTs were dispersed in 2-propanol and drop-casted on the monolayer graphene. Electric contacts were made by evaporation of gold onto a graphene SiO_2/Si substrate with a shadow mask. In the voltage gating experiment, the Pt/Ir coated probe tip and graphene were electrically grounded. A voltage was applied to the Si under the SiO_2 coating by a contact voltage source.

Experimental Methods. The near-field apparatus consisted of an atomic force microscope (Multimode AFM, Bruker Nano), tunable mid-infrared quantum cascade laser (QCL, Daylight Solutions), and supporting optics. Mid-infrared lasers (50 mW) were provided by the QCL and guided to the tip and sample region of the atomic force microscope. A metal-coated probe tip (DPE-14 Micromash) was used to enhance the light field at its apex through near field localization. The AFM operated in tapping mode with the tip oscillating vertically above the sample at Ω = 137 kHz with amplitude of 30 nm. The mid-infrared laser light was focused to and collected from the tip and sample region with a parabolic mirror with an effective numerical aperture of 0.24. The collimated scattered light was interferometrically homodyned with a reference laser field from the same source. An infrared detector (J15D12, Teledyne-Judson) was used to convert optical field into electric signal that was then demodulated by a lock-in amplifier (HF2Li Zurich instrument) at the third harmonic of the tip tapping frequency (3Ω). The $\pi/2$ homodyne phase condition was set by minimizing the near-field signal from the substrate, a procedure described in detail in the literature.[39] The in-phase homodyne condition was set by maximizing the near-field signal from the substrate. The spatial resolution of the near-field apparatus was measured to be ca. 10 nm.

Conflict of Interest: The authors declare no competing financial interest.

Acknowledgment. We thank Dr. Pierre Berini, Dr. Behnood G. Ghamsari, and Dr. Anjan Reijinders for helpful discussions. We thank Dr. Gregory O. Andreev for support with the instrumentation. This work was supported by NSERC. BNNT synthetic work was supported by the WPI-MANA Centre of NIMS, Tsukuba, Japan. D.G. also acknowledges financial support from a Grant-in-Aid for Scientific Research No. 26289244 (MEXT, Japan).

Supporting Information Available: Off-resonant s-SNOM images of BNNT on graphene, s-SNOM images showing graphene plasmons from boundaries, Fourier transform infrared spectrum of BNNTs, FDTD simulation of BNNT/graphene/SiO_2 structures, and graphene dielectric functions used in the simulations. This material is available free of charge *via* the Internet at http://pubs.acs.org.

REFERENCES AND NOTES

1. Maier, S. A. *Plasmonics: Fundamentals and Applications*; Springer: New York, 2007.
2. Ozbay, E. Plasmonics: Merging Photonics and Electronics at Nanoscale Dimensions. *Science* **2006**, *311*, 189–193.
3. Hillenbrand, R.; Taubner, T.; Keilmann, F. Phonon-Enhanced Light−Matter Interaction at the Nanometre Scale. *Nature* **2002**, *418*, 159–162.
4. Greffet, J.-J.; Carminati, R.; Joulain, K.; Mulet, J.-P.; Mainguy, S.; Chen, Y. Coherent Emission of Light by Thermal sources. *Nature* **2002**, *416*, 61–64.
5. Taubner, T.; Keilmann, F.; Hillenbrand, R. Nanomechanical Resonance Tuning and Phase Effects in Optical Near-Field Interaction. *Nano Lett.* **2004**, *4*, 1669–1672.
6. Korobkin, D.; Urzhumov, Y.; Neuner Iii, B.; Zorman, C.; Zhang, Z.; Mayergoyz, I.; Shvets, G. Mid-Infrared Metamaterial Based on Perforated SiC Membrane: Engineering Optical Response Using Surface Phonon Polaritons. *Appl. Phys. A: Mater. Sci. Process.* **2007**, *88*, 605–609.
7. Fonoberov, V. A.; Balandin, A. A. Polar Optical Phonons in Wurtzite Spheroidal Quantum Dots: Theory and Application to ZnO and ZnO/MgZnO Nanostructures. *J. Phys. Condens. Matter* **2005**, *17*, 1085.
8. Holmstrom, S. A.; Stievater, T. H.; Pruessner, M. W.; Park, D.; Rabinovich, W. S.; Khurgin, J. B.; Richardson, C. J.; Kanakaraju, S.; Calhoun, L. C.; Ghodssi, R. Guided-Mode Phonon-Polaritons in Suspended Waveguides. *Phys. Rev. B* **2012**, *86*, 165120.
9. Dai, S.; Fei, Z.; Ma, Q.; Rodin, A. S.; Wagner, M.; McLeod, A. S.; Liu, M. K.; Gannett, W.; Regan, W.; Watanabe, K.; *et al.* Tunable Phonon Polaritons in Atomically Thin van der Waals Crystals of Boron Nitride. *Science* **2014**, *343*, 1125–1129.
10. Brar, V. W.; Jang, M. S.; Sherrott, M.; Kim, S.; Lopez, J. J.; Kim, L. B.; Choi, M.; Atwater, H. Hybrid Surface-Phonon-Plasmon Polariton Modes in Graphene/Monolayer h-BN Heterostructures. *Nano Lett.* **2014**, *14*, 3876–80.
11. Caldwell, J. D.; Kretinin, A.; Chen, Y.; Giannini, V.; Fogler, M. M.; Francescato, Y.; Ellis, C. T.; Tischler, J. G.; Woods, C. R.; Giles, A. J., *et al.* Sub-diffraction, Volume-confined Polaritons in the Natural Hyperbolic Material, Hexagonal Boron Nitride. *arXiv Preprint* **2014**, arXiv:1404.0494.
12. Xu, X. G.; Ghamsari, B. G.; Jiang, J.-H.; Gilburd, L.; Andreev, G. O.; Zhi, C.; Bando, Y.; Golberg, D.; Berini, P.; Walker, G. C. One-Dimensional Surface Phonon Polaritons in Boron Nitride Nanotubes *Nat. Commun.* **2014**, *5*, 4782.
13. Caldwell, J. D.; Lindsay, L.; Giannini, V.; Vurgaftman, I.; Reinecke, T. L.; Maier, S. A.; Glembocki, O. J. Low-Loss, Infrared and Terahertz Nanophotonics Using Surface Phonon Polaritons. *Nanophotonics* **2014**, 10.1515/nanoph-2014-0003.
14. Zayats, A. V.; Smolyaninov, I. I.; Maradudin, A. A. Nano-optics of Surface Plasmon Polaritons. *Phys. Rep.* **2005**, *408*, 131–314.
15. Fei, Z.; Andreev, G. O.; Bao, W.; Zhang, L. M.; S. McLeod, A.; Wang, C.; Stewart, M. K.; Zhao, Z.; Dominguez, G.;

Thiemens, M.; *et al.* Infrared Nanoscopy of Dirac Plasmons at the Graphene−SiO_2 Interface. *Nano Lett.* **2011**, *11*, 4701–4705.
16. Koppens, F. H.; Chang, D. E.; Garcia de Abajo, F. J. Graphene Plasmonics: a Platform for Strong Light−Matter Interactions. *Nano Lett.* **2011**, *11*, 3370–3377.
17. Chen, J.; Badioli, M.; Alonso-González, P.; Thongrattanasiri, S.; Huth, F.; Osmond, J.; Spasenović, M.; Centeno, A.; Pesquera, A.; Godignon, P.; *et al.* Optical Nano-imaging of Gate-Tunable Graphene Plasmons. *Nature* **2012**, *487*, 77–81.
18. Fei, Z.; Rodin, A. S.; Andreev, G. O.; Bao, W.; McLeod, A. S.; Wagner, M.; Zhang, L. M.; Zhao, Z.; Thiemens, M.; Dominguez, G.; *et al.* Gate-Tuning of Graphene Plasmons Revealed by Infrared Nano-imaging. *Nature* **2012**, *487*, 5.
19. Novoselov, K.; Geim, A. K.; Morozov, S.; Jiang, D.; Grigorieva, M. K. I.; Dubonos, S.; Firsov, A. Two-dimensional Gas of Massless Dirac Fermions in Graphene. *Nature* **2005**, *438*, 197–200.
20. Chopra, N. G.; Luyken, R.; Cherrey, K.; Crespi, V. H.; Cohen, M. L.; Louie, S. G.; Zettl, A. Boron Nitride Nanotubes. *Science* **1995**, *269*, 966–967.
21. Shi, Y.; Hamsen, C.; Jia, X.; Kim, K. K.; Reina, A.; Hofmann, M.; Hsu, A. L.; Zhang, K.; Li, H.; Juang, Z.-Y.; *et al.* Synthesis of Few-layer Hexagonal Boron Nitride Thin Film by Chemical Vapor Deposition. *Nano Lett.* **2010**, *10*, 4134–4139.
22. Matsuda, T.; Uno, N.; Nakae, H.; Hirai, T. Synthesis and Structure of Chemically Vapour-Deposited Boron Nitride. *J. Mater. Sci.* **1986**, *21*, 649–658.
23. Geick, R.; Perry, C. H.; Rupprecht, G. Normal Modes in Hexagonal Boron Nitride. *Phys. Rev.* **1966**, *146*, 543–547.
24. Zhi, C.; Xu, Y.; Bando, Y.; Golberg, D. Highly Thermoconductive Fluid with Boron Nitride Nanofillers. *ACS Nano* **2011**, *5*, 6571–6577.
25. Ciofani, G.; Danti, S.; D'Alessandro, D.; Ricotti, L.; Moscato, S.; Bertoni, G.; Falqui, A.; Berrettini, S.; Petrini, M.; Mattoli, V.; *et al.* Enhancement of Neurite Outgrowth in Neuronal-Like Cells Following Boron Nitride Nanotube-Mediated Stimulation. *ACS Nano* **2010**, *4*, 6267–6277.
26. Golberg, D.; Bando, Y.; Huang, Y.; Terao, T.; Mitome, M.; Tang, C. C.; Zhi, C. Y. Boron Nitride Nanotubes and Nanosheets. *ACS Nano* **2010**, *4*, 2979–2993.
27. Reddy, A. L. M.; Srivastava, A.; Gowda, S. R.; Gullapalli, H.; Dubey, M.; Ajayan, P. M. Synthesis of Nitrogen-Doped Graphene Films for Lithium Battery Application. *ACS Nano* **2010**, *4*, 6337–6342.
28. Pakdel, A.; Zhi, C.; Bando, Y.; Nakayama, T.; Golberg, D. Boron Nitride Nanosheet Coatings with Controllable Water Repellency. *ACS Nano* **2011**, *5*, 6507–6515.
29. Brar, V. W.; Jang, M. S.; Sherrott, M.; Lopez, J. J.; Atwater, H. A. Highly Confined Tunable Mid-infrared Plasmonics in Graphene Nanoresonators. *Nano Lett.* **2013**, *13*, 2541–2547.
30. Yan, H.; Low, T.; Zhu, W.; Wu, Y.; Freitag, M.; Li, X.; Guinea, F.; Avouris, P.; Xia, F. Damping Pathways of Mid-infrared Plasmons in Graphene Nanostructures. *Nat. Photonics* **2013**, *7*, 394–399.
31. Liu, Y.; Willis, R. F. Plasmon-Phonon Strongly Coupled Mode in Epitaxial Graphene. *Phys. Rev. B* **2010**, *81*, 081406.
32. Koch, R. J.; Seyller, T.; Schaefer, J. A. Strong Phonon-Plasmon Coupled Modes in the Graphene/Silicon Carbide Heterosystem. *Phys. Rev. B* **2010**, *82*, 201413.
33. Schnell, M.; Garcia-Etxarri, A.; Huber, A.; Crozier, K.; Aizpurua, J.; Hillenbrand, R. Controlling the Near-Field Oscillations of Loaded Plasmonic Nanoantennas. *Nat. Photonics* **2009**, *3*, 287–291.
34. Stiegler, J. M.; Abate, Y.; Cvitkovic, A.; Romanyuk, Y. E.; Huber, A. J.; Leone, S. R.; Hillenbrand, R. Nanoscale Infrared Absorption Spectroscopy of Individual Nanoparticles Enabled by Scattering-Type Near-field Microscopy. *ACS Nano* **2011**, *5*, 6494–6499.
35. Ocelic, N.; Hillenbrand, R. Subwavelength-Scale Tailoring of Surface Phonon Polaritons by Focused Ion-Beam Implantation. *Nat. Mater.* **2004**, *3*, 606–609.
36. Zhi, C.; Bando, Y.; Tan, C. C.; Golberg, D. Effective Precursor for High Yield Synthesis of Pure BN Nanotubes. *Solid State Commun.* **2005**, *135*, 67–70.
37. Watanabe, K.; Taniguchi, T.; Kanda, H. Direct-Bandgap Properties and Evidence for Ultraviolet Lasing of Hexagonal Boron Nitride Single Crystal. *Nat. Mater.* **2004**, *3*, 404–409.
38. Taniguchi, T.; Watanabe, K. Synthesis of High-Purity Boron Nitride Single Crystals under High Pressure by Using Ba−BN Solvent. *J. Cryst. Growth* **2007**, *303*, 525–529.
39. Xu, X. G.; Tanur, A. E.; Walker, G. C. Phase Controlled Homodyne Infrared Near-Field Microscopy and Spectroscopy Reveal Inhomogeneity within and among Individual Boron Nitride Nanotubes. *J. Phys. Chem. A* **2013**, *117*, 3348–3354.
40. Fakrach, B.; Rahmani, A.; Chadli, H.; Sbai, K.; Bentaleb, M.; Bantignies, J.-L.; Sauvajol, J.-L. Infrared Spectrum of Single-Walled Boron Nitride Nanotubes. *Phys. Rev. B* **2012**, *85*, 115437.
41. Hwang, E.; Sarma, S. D. Dielectric Function, Screening, and Plasmons in Two-dimensional Graphene. *Phys. Rev. B* **2007**, *75*, 205418.
42. Dean, C. R.; Young, A. F.; Meric, I.; Lee, C.; Wang, L.; Sorgenfrei, S.; Watanabe, K.; Taniguchi, T.; Kim, P.; Shepard, K. L.; *et al.* Boron Nitride Substrates for High-Quality Graphene Electronics. *Nat. Nanotechnol.* **2010**, *5*, 722–726.
43. Levendorf, M. P.; Kim, C.-J.; Brown, L.; Huang, P. Y.; Havener, R. W.; Muller, D. A.; Park, J. Graphene and Boron Nitride Lateral Heterostructures for Atomically Thin Circuitry. *Nature* **2012**, *488*, 627–632.
44. Bresnehan, M. S.; Hollander, M. J.; Wetherington, M.; LaBella, M.; Trumbull, K. A.; Cavalero, R.; Snyder, D. W.; Robinson, J. A. Integration of Hexagonal Boron Nitride with Quasi-freestanding Epitaxial Graphene: Toward Wafer-Scale, High-Performance Devices. *ACS Nano* **2012**, *6*, 5234–5241.
45. Kim, K. K.; Hsu, A.; Jia, X.; Kim, S. M.; Shi, Y.; Dresselhaus, M.; Palacios, T.; Kong, J. Synthesis and Characterization of Hexagonal Boron Nitride Film as a Dielectric Layer for Graphene Devices. *ACS Nano* **2012**, *6*, 8583–8590.